



ELSEVIER

Available online at www.sciencedirect.com

SCIENCE @ DIRECT®

Journal of Volcanology and Geothermal Research 135 (2004) 51–73

Journal of volcanology
and geothermal research

www.elsevier.com/locate/jvolgeores

Integrated satellite observations of the 2001 eruption of Mt. Cleveland, Alaska

Kenneson G. Dean*, Jonathan Dehn, Kenneth R. Papp, Steve Smith, Pavel Izbekov, Rorik Peterson, Courtney Kearney, Andrea Steffke

Geophysical Institute, University of Alaska Fairbanks, P.O. Box 757320, Fairbanks, AK, USA

Accepted 5 December 2003

Abstract

Satellite data were the primary source of information for the eruption of Mt. Cleveland, Alaska on 19 February, and 11 and 19 March 2001. Multiple data sets were used pre-, syn- and post-eruption to mitigate the hazard and determine an eruption chronology. The 19 February eruption was the largest of the three, resulting in a volcanic cloud that formed an arc over 1000 km long, moved to the NE across Alaska and was tracked using satellite data over more than a 50-h period. The volcanic cloud was “concurrently” detected on the GOES, AVHRR and MODIS data at various times and their respective signals compared. All three sensors detected a cloud that had a very similar shape and position but there were differences in their areal extent and internal structural detail. GOES data showed the largest volcanic cloud in terms of area, probably due to its oblique geometry. MODIS bands 31 and 32, which are comparable to GOES and AVHRR thermal infrared wavelengths, were the least effective single channels at detecting the volcanic cloud of those investigated (MODIS bands 28, 29, 31 and 32). MODIS bands 28 and 29 detected the largest volcanic clouds that could easily be distinguished from weather clouds. Of the split-window data, MODIS bands 29 minus band 32 detected the largest cloud, but the band 31 minus band 32 data showed the volcanic cloud with the most internal structural detail. The Puff tracking model accurately tracked the movement, and predicted the extent and shape of this complex cloud even into areas beyond satellite detection. Numerous thermal anomalies were also observed during the eruption on the twice-daily AVHRR data and the high spatial-resolution Landsat data. The high-resolution Radarsat data showed that the AVHRR thermal anomalies were due to lava and debris flow features and a newly formed fan along the west coast of the island. Field observations and images from a hand-held Forward Looking Infrared Radiometer (FLIR) showed that the flow features were a lava, debris flows and a warm debris fan along the west coast. Real-time satellite data were the primary tool used to monitor the eruption, track changes and to mitigate hazards. High-resolution data, even though coverage is infrequent, were critical in helping to identify volcanic processes and to compile an eruption chronology.

© 2004 Elsevier B.V. All rights reserved.

Keywords: Mt. Cleveland; remote sensing; MODIS; volcanic ash cloud

1. Introduction

The goal of this research is to present an analysis of the chronology and volcanic processes of the 2001 eruption of Mt. Cleveland Volcano, Alaska using data

* Corresponding author.

E-mail address: ken.dean@gi.alaska.edu (K.G. Dean).

from Geostationary Operational Environmental Satellite (GOES), Advanced Very High Resolution Radiometer (AVHRR), Moderate Resolution Imaging Radiometer (MODIS), Landsat and Radarsat data. The eruption was somewhat unique in the North Pacific Region in that only satellite data were available to monitor and assess the activity. Mt. Cleveland erupted explosively on 19 February (the largest in terms of volume and energy of the eruption) and on 11 and 19 March 2001. The eruption on 19 February was unique in three respects: (1) the February event produced a unusually long arcing ash cloud that drifted to the northeast across most of Alaska; (2) the position of the cloud was detected on GOES satellite data for several days at very high latitudes; and (3) the eruption was recorded on numerous satellite data sets including those from the new Earth Observations Systems (EOS) satellite sensors. These data, in conjunction with field observations, made it possible to analyze the events that led up to the eruption, create an eruption chronology, and study the volcanic processes and development of new landforms.

Mt. Cleveland is located on the western half of Chuginadak Island, which is part of the Islands of Four Mountains group located in the east–central Aleutian Islands, Alaska. Chuginadak Island is uninhabited and remote, located 1526 km southwest of Anchorage. The closest inhabited community, Nikolski, is 75 km to the east on Umnak Island (Fig. 1). The volcano is a

distinctively conical, young stratovolcano, 1730 m in elevation with steep slopes. At sea level, the base of the cone is approximately 8 km across, suggesting a volcanic cone volume above sea level of about 29 km^3 . The cone is completely undissected, suggesting that much of the exposed volcano is Holocene in age. Mt. Cleveland has erupted at least 11 times since 1893 (Miller et al., 1998). These eruptions have been characterized by short-lived explosive bursts of ash that were accompanied by lava fountaining and lava flows. Prior to the 2001 eruption, the most recent activity was a short-lived ash volcanic cloud that rose to an altitude of approximately 10 km on 25 May 1994 (Neal et al., 1995). Mt. Cleveland is not yet monitored with seismic or other geophysical instruments, and no geologic mapping or chemical analyses of lava and pyroclastic deposits existed prior to 2001/2002 when field parties investigated the products of the 2001 eruption. Aerial photographs had, however, revealed many young, leveled lava flows and debris fans with varying types of vegetative cover that form an essentially continuous apron around the cone.

2. Background

The 40 historically active volcanoes in Alaska are monitored by the Alaska Volcano Observatory (AVO) in real or near real-time using satellite (Dean et al.,

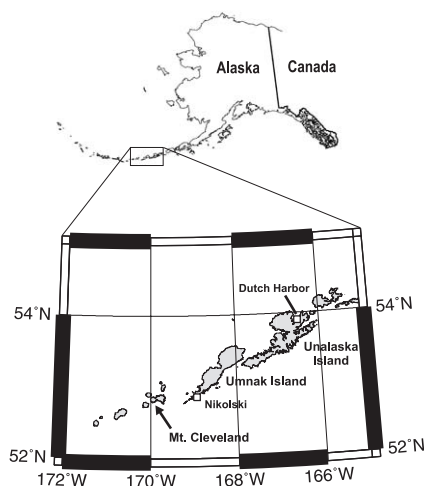


Fig. 1. Mt. Cleveland, a 1730-m tall stratovolcano, is located on the western end of Chuginadak Island, approximately 70 km west of the town of Nikolski in the central Aleutian Islands. It is one of the Islands of Four Mountains and the most active volcano of this group.

2002; Schneider et al., 2000) or geophysical techniques (McNutt, 1996). In addition, observers on the ground and in the air report anomalous activity. Satellite or airborne data compliment geophysical and geological techniques in that they record surface phenomena, such as elevated surface temperatures, volcanic clouds and changes in the landscape. In recent years, the role of satellite monitoring at AVO has changed from this complimentary role to become a prime means of hazard detection, particularly at volcanoes where no other geophysical techniques have been, or can be, applied. Being the only tool available at Cleveland Volcano (Dean et al., 2002), the 2001 eruption of Mt. Cleveland is a good example of volcanic activity detected and monitored using satellite imagery. The most critical hazards that result from the eruption of most other Alaskan volcanoes, including Mt. Cleveland, are related primarily to airborne ash due to its potential damage to aircraft in the region (Schneider et al., 2000).

Satellite observations of elevated surface temperatures at active volcanoes have become an important component for monitoring volcanoes (Harris et al., 1997, 2000; Dehn et al., 2000). Ground temperature and heat flux can be calculated when the geometry of the anomalous area relative to a background signal is known (Harris et al., 1997). Based on this research, models for detecting hot ground has been developed (Higgins and Harris, 1997; Dean et al., 1998). After an eruption has begun, data from the ASTER and Landsat 7 sensors have provided new insight into the structure of lava domes and flows (Flynn et al., 2000; Harris et al., 2003; Ramsey and Dehn, 2003). These data are useful during the crisis to help determine potential hazards that may arise during an eruption (such as lava dome instability) and to analyze eruption processes post-crisis (Flynn et al., 2000; Ramsey and Dehn, 2003).

GOES and AVHRR satellite data are accepted tools for detecting and monitoring volcanic clouds (e.g. Carn and Oppenheimer, 2000; Hufford et al., 2000; Schneider et al., 2000; Dean et al., 2002). Techniques have been developed to detect ash clouds by subtracting or ratioing long-wave thermal-infrared bands, referred to as the split-window technique (Prata, 1989; Holasek and Rose, 1991). However, not all of the detection techniques are 100% successful (Schneider et al., 1995; Prata et al., 2001; Simpson

et al., 2000). Ash retrieval models have been developed to estimate ash particle size and total mass (Rose and Mayberry, 2000; Rose et al., 2001; Wen and Rose, 1994; Schneider et al., 1999). The effects of particle size, composition, cloud opacity and atmospheric parameters, such as amount of water vapor and icing, on the signal in split-window imagery have been modeled (Rose et al., 1995, 2001; Yu and Rose, 2002). The ash retrieval models also give a rough estimate of the detection limit and how much volcanic ash is needed for a split-window signal to become detectable. The split-window technique has become a useful monitoring tool in the arctic and sub-arctic in a relative sense, i.e. whether there has been an increase or decrease in the strength of the split-window signal compared to the previous image. To further aid in the mitigation of hazards from eruption clouds, dispersion models have been developed to predict the movement and structure of volcanic clouds, particularly when no satellite image is available, or where satellite imagery may not detect the cloud (Heffter and Stunder, 1993; Searcy et al., 1998; D'Amours, 1998). These models allow us to predict the position and relative concentration of ash particles of volcanic ash. Puff and other dispersion models rely on three-dimensional gridded wind fields for regional or global predictions. The accuracy of these models are controlled by the accuracy of the forecast wind data and can be evaluated by comparing the simulations with satellite images of eruption clouds (Searcy et al., 1998). Satellite data are critical to simulations, because the type and accuracy of input information and wind fields vary with each eruption and will affect the results.

3. Satellite data

Satellite data used in the analysis of the 2001 eruption of Mt. Cleveland are GOES, AVHRR, MODIS, Landsat and Radarsat data (Table 1). Each of these instruments records data at different wavelengths (e.g. visible to thermal to microwave), at different spatial resolutions (15 m to 8 km at this latitude), and with temporal resolution ranging from every 15 min to 24 days. GOES and AVHRR data were available in real-time during the 2001 eruptions.

MODIS was a new sensor at this time, flown on the Terra satellite and used for volcano monitoring, but

Table 1
List of satellite data used in the analysis of the eruption of Mt. Cleveland

Satellite (all polar orbit except GOES)	Bands	Wavelengths (μm)	Spatial resolution	Repeat coverage
GOES (Geostationary)	B 4	10.5–11.5	8.0 km at	0.5 h
	B 5	11.5–12.5	60 N	
AVHRR	B 4	10.3–11.3	1.1 km at	Every few hours at 60 N/satellite due to large swath width and overlap
	B 5	11.4–12.4	nadir	
MODIS	B 28	7.175–7.475	1.0 km at	Every few hours at 60 N/satellite due to large swath width and overlap
	B 29	8.4–8.7	nadir	
Landsat	B 31	10.78–11.28		16 days
	B 32	11.77–12.27		
	B 2	0.53–0.61	30 m	
	B 4	0.78–0.90	30 m	
Radarsat	B 5	1.55–1.75	30 m	14 days
	B 6	10.4–12.5	630 m	
	C Band	5.6 cm	30 m (std. beam)	

was not yet available in real-time to AVO during the Cleveland eruption. AVO began using MODIS data for operational monitoring in 2002.

In this paper the various bands of satellite data will be referred to as B4 with the number indicating the channel number. The split-window bands will be referred to using “m” indicating minus, such as B4m5.

4. Eruption chronology

The first indication to AVO of new activity at Mt. Cleveland was the 19 February eruption itself. However, after the eruption, AVO received reports indicating that precursory activity had taken place. Most graphic of this evidence was a photograph taken on 2 February by a pilot flying near the volcano showing a dark, lobate deposit on the snow-covered southwest flank and robust steaming from the summit crater. An

International Space Station image recorded a month previously showed a snow-covered stratocone, unmarked by ash, lava or debris. During this same period, residents of Nikolski, located 70 km east of the volcano, observed steaming at the summit and snowmelt on the flanks of the cone. Later analysis of AVHRR and MODIS satellite imagery revealed faint thermal anomalies on the 9th and 12th February, respectively. These anomalies were located at the summit and of low thermal contrast (less than 5 °C above background in integrated pixel temperature) and difficult to detect during the course of regular monitoring, and were thus overlooked preceding the eruption.

5. Drifting volcanic clouds

On 19 February, Mt. Cleveland erupted explosively for at least 8 h, starting at approximately 1430 and ending between 2230 and 0242 UT the following day based on GOES satellite observations. The GOES satellite data showed that the volcanic cloud disconnected from the volcano between 2315 and 0242 UT, although a decrease in seismic signals at 2230 UT detected by instruments at Makushin Volcano, 230 km away suggest that the eruption may have stopped prior to that time. Pilot reports indicate that the altitude of the volcanic cloud increased with time from 7.5 km a few hours after the start of the eruption and up to 12 km 8 h later.

The volcanic cloud and a thermal anomaly were detected in the first post-eruption AVHRR satellite data recorded at 1655 UT (Fig. 2). The cloud was complex and extended in two directions, 40 km northwest and 60 km southeast of the volcano. The SE volcanic cloud extends further from the volcano and was more defuse than the NE volcanic cloud, and hence may have been slightly older. Initial observations using single channel data detected only the northwest cloud, which had a brightness temperature of -53 °C that correlated to an altitude of 8 km based on the atmospheric temperature profile at that time. Further analysis, using the split-window technique (in this case B4m5 in AVHRR) Prata (1989) showed that there was another portion of the volcanic cloud extending to the southeast. The translucent SE cloud had a strong split-window ash signal (-4.9) but the

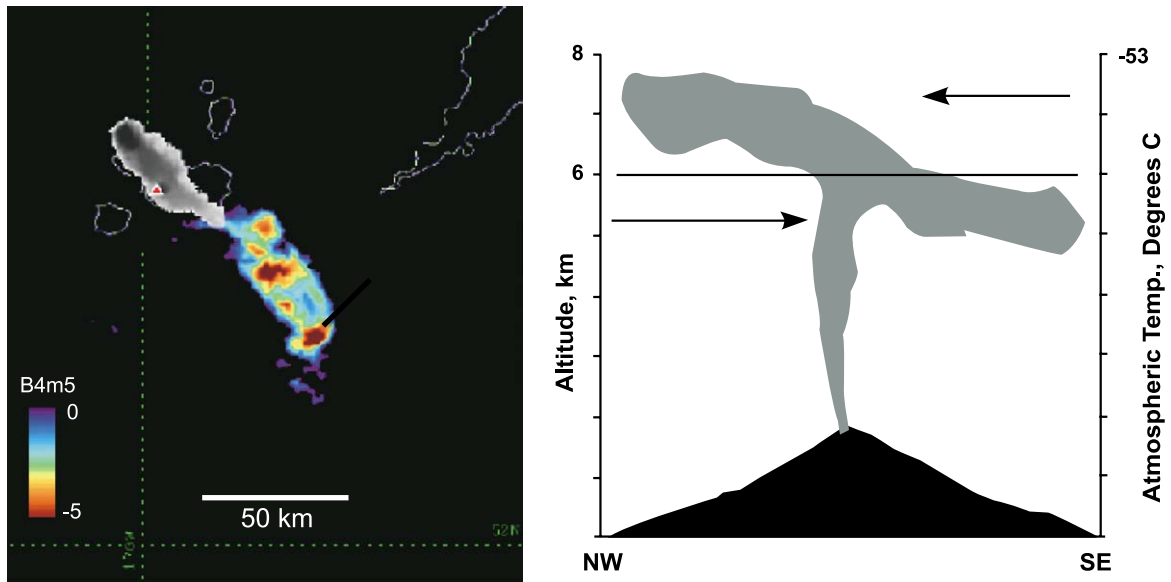


Fig. 2. An AVHRR satellite image (left) and conceptual model (right) show an early stage of the volcanic cloud at 1655 UT. The NW portion was opaque and detected on single channel thermal infrared (TIR) B4 data with a radiant temperature of -53°C , which correlates to an altitude of 8 km. The SE volcanic cloud was semi-transparent and detected on B4m5 data. A wind shear detected using the Puff dispersion model indicated the SE volcanic cloud to be below approximately 6 km altitude.

northwest cloud, though laden with ash (as shown on succeeding images), had a weak split-window signal (-1.8) at this time, presumably due to its high opacity. Wind direction and velocities indicate that the SE volcanic cloud was lower in altitude. The Puff ash dispersion model showed a wind shear at a height of approximately 6 km, suggesting that the SE cloud was below this altitude. The wind shear caused the early bifurcation of the volcanic cloud resulting in the NW and SE extension; however, the overall drift of the volcanic cloud was to the northeast. A few hours later (about 2115 UT) dacitic ash fell at the town of Nikolski, 75 km from the summit.

The volcano erupted into an atmospheric deformation zone between a low-pressure system to the southeast, and a front moving to the northeast. As a result, the ash cloud became an elongated arc moving to the northeast over the Alaska Peninsula and across the Alaska mainland. It was easily detected for 48 h on time sequential GOES split-window data (Dean et al., 2002). By 21 February (0300 UT), 35 h after the eruption, the ash cloud was more than 1000 km long and extended from Cook Inlet, Alaska, to Chukotsk Peninsula, Russia. An animation of GOES B4m5 data

showed that eventually this long, arcing cloud split into three segments that drifted north over the Arctic Ocean, over Fairbanks near the center of the state and south over the Gulf of Alaska. After 21 February, 1930 UT, the Fairbanks and Gulf of Alaska segments were pulled into a low pressure system in the southern Gulf of Alaska and became too diffuse or masked by weather clouds to be detected in the GOES data. The volcanic cloud was observed and reported by many pilots throughout its long traverse (Dean et al., 2002), and had a significant effect on air traffic in the region, with nearly 40 known flight cancellations, diversions or delays.

Mt. Cleveland erupted explosively again on 11 March. This eruption was much smaller than the 19 February event, lasting 3 h (1330–1700 UT) based on GOES and AVHRR satellite observations, with an estimated maximum cloud height of 8 km. Split-window data showed ash extending from 600 to 760 km east of Mt. Cleveland on 12 March, 2230 UT. These clouds drifted northeast over 1000 km until they fell below detection thresholds near Kodiak Island after about 42 h on 13 March. No significant effect on air traffic was reported.

The last explosive eruption came on 19 March lasting up to 6 h (2330–0530 UT) based on GOES data with an estimated cloud height of up to 9 km according to the National Weather Service. AVHRR data recorded at 0330 UTC on 20 March showed a fan-shaped volcanic cloud with the apex at the volcano and facing southeast. The volcanic cloud was still attached to the volcano at this time. A strong ash signal was detected in the northern leg of the cloud in the AVHRR split-window data. At the time of the image the cloud extended approximately 200 km from the volcano. South- and east-drifting ash clouds were detected in GOES split-window images for about 9 h. An observer in Nikolski reported a strong haze, but no ash fall was observed in the town. The volcanic cloud was observed by pilots, but no severe interruption of air traffic was reported. Additional thermal anomalies were observed at the volcano throughout March and April, though no more sub-Plinian explosive activity was observed.

6. Ash fall at Nikolski

Despite the extensive area traversed by the February volcanic-cloud, an observed ash fall was reported only at the town of Nikolski, 75 km northeast of the volcano. The ash fall started at 2115 UT and lasted approximately 5 h but only resulted in a very light dusting. This ash was airborne for about 7 h before falling at Nikolski. The time of the ash fall coincides with the ash rich portion of the cloud passing overhead as determined by the strongest split-window signal in the MODIS (2310 UT) and GOES (2315 UT) satellite data, as well as the Puff tracking model.

Analysis of the ash collected at Nikolski showed that it was composed of glass shards, crystals and lithics. The median grain size is 54 μm and well-sorted, containing 70.4% fines (ash <63 μm). Glass shards make up more than 90% of the deposit. The glass is dacitic and with a magmatic morphology rather than phreatomagmatic, i.e. bubble-wall and vesicular shards as compared to blocky and vesicle poor shards. The crystals are plagioclase (dominant phase), orthopyroxene, clinopyroxene and Ti-magnetite. Lithics are mainly vesicular scoria (P. Izbekov, B. Browne, J. Gardner, AVO, pers. commun., 2001).

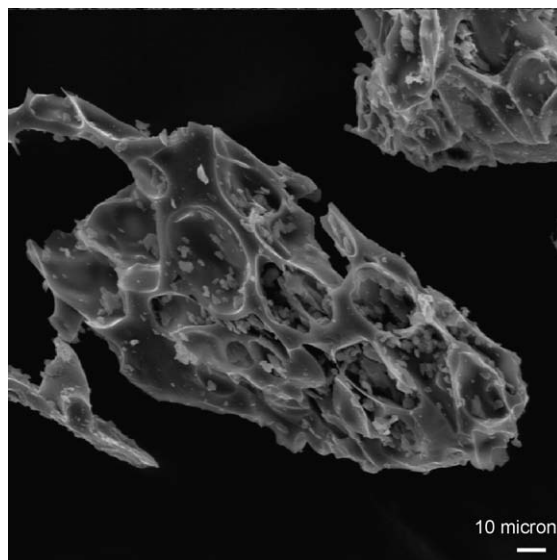


Fig. 3. Scanning electron microscope (SEM) microgram of ash that fell at Nikolski. The ash is composed mostly of glass shards, crystals and lithics with a median grain size of 54 μm . It is well-sorted, containing 70.4% fines (ash <63 μm). The ash particles are elongated, sub-angular and vesicular. The sample represents ash that was airborne for 5.25 h, and detected on GOES, AVHRR and MODIS data.

The size and shape of the Nikolski ash were well within the range best detected in the split-window algorithm, i.e. fine dry ash with a significant volume fraction less than 20 microns in size (Wen and Rose, 1994). Scanning Electron Microscope micrograms (Fig. 3) showed that the ash particles were elongated, sub-angular and vesicular, which are important parameters to consider when modeling dispersion and fall-out. Ash that did not fall at Nikolski continued to drift to the NE as observed on the satellite data, and probably included a higher concentration of even finer grained particles. The volcanic cloud was detected on GOES and MODIS satellite data for the next 2 days.

7. Comparison of volcanic clouds on multiple data sets (19 February eruption)

Three days of satellite observations of the 19 February ash cloud made this an ideal situation to compare the capabilities of GOES, AVHRR and MODIS sensors to detect volcanic clouds at high

latitudes (Table 2). Multiple data sets were recorded during the first 12 h of the eruption that were approximately concurrent in time and hence were selected for analysis. This time period is divided into early, mid and late periods of observations. In the

Early Period GOES and AVHRR data are recorded within 28 min of each other, in the Mid Period MODIS and GOES data are within 5 min of each other, and in the Late Period AVHRR and GOES data are recorded within 12 min of each other. For consis-

Table 2
Characteristics and areal measurements of volcanic cloud observed on each data set

Sensor/date/image name	Band	Wavelength (μm)	Spatial resolution (km)		Volcanic cloud area volcanic cloud (km^2)	Comments
			Nadir	Corrected		
<i>Early Period (+1.45 h since the start of the eruption)</i>						
GOES 19 February 2001 1615 UT	4	10.2–11.2	4.0	5.0–6.0	1050	Difficult to distinguish the cloud <100 pixels
20010219.1615.lo.g10.lo.reg	4m5	Approx. 10–12	4.0	5.0–6.0	2450	
AVHRR 19 February 2001 1643 UT	4	10.3–11.3	1.1	1.1	1300	Mostly opaque volcanic cloud to NW Stronger signal to SE weak signal to NW
n14.01050.1643	4m5	Approx. 10–12	1.1	1.1	1950	
<i>Mid Period (+8.45 h since the start of the eruption)</i>						
MODIS 19 February 2001 2310 UT	28	7.175–7.475	1.0	1.5–2.5	6100	Distinct volcanic cloud to NE and then NW
MOD021KM	29	8.4–8.7	1.0	1.5–2.5	6200	
A2001050.2310.003.2001.360174728						Similar to B28 but brighter and distinct
	31	10.78–11.28	1.0	1.5–2.5	4500	Similar to B28 and 29 but weaker signal
	32	11.77–12.27	1.0	1.5–2.5	4100	Weakest signal of the four bands analyzed
	28m32	B 28–B 32	1.0	1.5–2.5	3400	Only detected small portion of cloud near volcano, SO_2 ?
	29m32	B 29–B 32	1.0	1.5–2.5	13,100	Detects broadest volcanic cloud, may include SO_2 and some weather clouds
	31m32	B 31–B 32	1.0	1.5–2.5	9300	Distinct volcanic cloud drifting to NE and extending to NW, shows more internal structure than 29m32
GOES 19 February 2001 2315 UT	4	10.2–11.2	4.0	5.0–6.0	13,000	Distinct volcanic cloud drifting to NE and extending to NW
20010219.2315.lo.g10.lo.reg	4m5	Approx. 10–12	4.0	5.0–6.0	11,800	
						Distinct volcanic cloud drifting to NE and extending to NW
<i>Late Period (+12 h since the start of the eruption)</i>						
GOES 20 February 2001 0230 UT	4	10.2–11.2	4.0	5.0–6.0	23,300	Translucent cloud disconnected from volcano and drifting NW and NE
20010220.0230.lo.g10.lo.reg	4m5	Approx. 10–12	4.0	5.0–6.0	9550	
						Volcanic cloud disconnected from volcano but easily detected with some internal structure
AVHRR 20 February 2001 0242 UT	4	10.3–11.3	1.1	1.3–1.4	26,850	Translucent cloud difficult to distinguish from weather clouds
N14.01051.0242	4m5	Approx. 10–12	1.1	1.3–1.4	16,250	
						Volcanic cloud easily detected with internal structure

tency, we only use MODIS B31 and B32 for comparison with other data because they are approximately equivalent to the spectral range of AVHRR and GOES B4 and B5. During the Mid Period, we also compare the signature of the volcanic cloud detected on MODIS channels 28, 29, 31 and 32.

Our analysis consists of comparing the area and structure of the volcanic cloud detected on single and split-window bands in thermal infrared (TIR) wavelength range, approximately 7–12 μm , and a qualitative assessment of volcanic cloud morphology. Each data set was analyzed using similar processing parameters, consisting of sub-sectioning, correcting geometry and optimizing the extent of the volcanic cloud

based on its radiometric response. All of the data were mapped to Albers Equal Projection. For area comparisons the volcanic cloud was manually delineated on each image and the area calculated. The delineation is somewhat qualitative and thus a potential source of error. Split-window values are presented for qualitative comparisons. A quantitative comparison of the split-window values is beyond the scope of this paper since it will require a more in-depth study due to the varying complex set of volcanic, environmental and orbital conditions (Schneider et al., 1999) associated with this signal.

The volcanic cloud from the Early Period (Fig. 4), 1.75 h after the start of the eruption, was recorded by

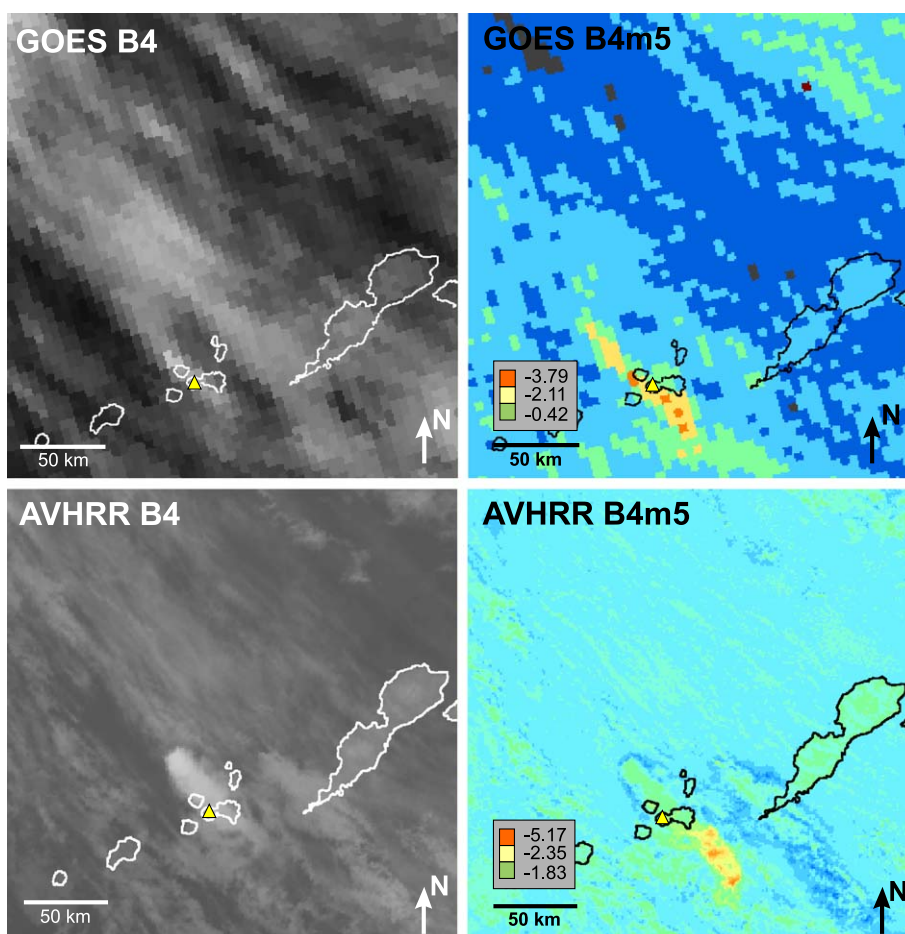


Fig. 4. GOES (1615 UT) and AVHRR (1643 UT) satellite images recorded approximately 2 h after the start of the 19 February 2001 eruption. These images were recorded within 28 min of each other. The volcanic cloud is faint on the GOES data, but 28 min later it is clearly evident on the AVHRR data. AVHRR B4 only detects the NW opaque volcanic cloud and the B4m5 only shows the SW translucent cloud.

GOES (1615 UT) and AVHRR (1643 UT) data. The cloud on the AVHRR data has drifted to the NE. The cloud in the GOES B4 data occupies only a few pixels (<100) and is faint and not clearly distinguishable from surrounding weather clouds. The GOES B4m5 cloud extends NW and SE of the volcano with lowest B4m5 value of -3.8 . Thirty minutes later, the volcanic cloud on the AVHRR B4 and B4m5 images are easily distinguished from weather clouds. The volcanic cloud in the AVHRR and GOES split-window data is about the same total area but the AVHRR has the strongest B4m5 signal (-5.2). The NW segment of the cloud has a slightly stronger GOES B4m5 signal although the AVHRR signal is more difficult to

distinguish from surrounding weather clouds. Generally, both split-window images detect the strongest B4m5 signals in about the same location after accounting for the NE drift of the cloud. The area of the detected cloud in the split-window data was approximately twice the area of the B4 data.

The volcanic cloud from the Mid Period (Fig. 5) was recorded by MODIS (2310 UT) and GOES (2315 UT) data approximately 9 h after the start of the eruption and only 5 min apart. The volcanic cloud was still connected to the volcano at this time. Data from both sensors detected a volcanic cloud that looked surprisingly similar in shape and size despite the differences in spatial resolution (MODIS ~ 1 km

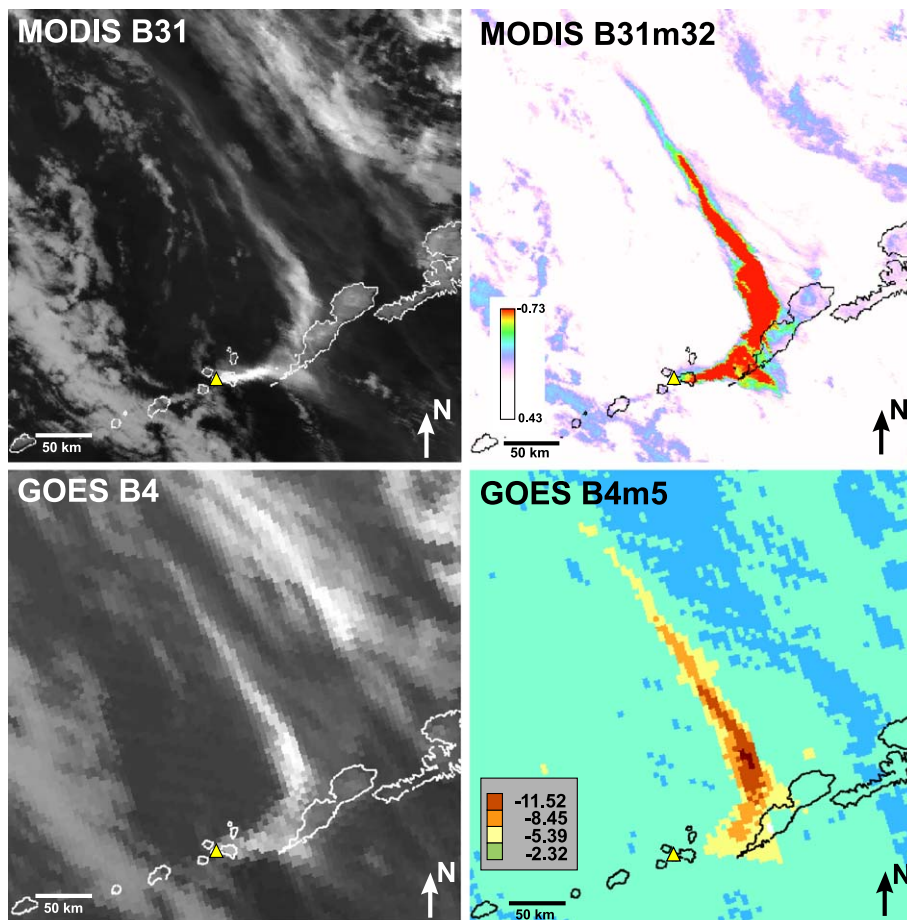


Fig. 5. MODIS (2310 UT) and GOES (2315 UT) satellite images recorded approximately 9 h after the start of the 19 February 2001 eruption. These images are recorded in the 10–12 μm range within 5 min of each other. Notice how similar the volcanic clouds are even though GOES data has much coarser resolution and oblique zenith angle ($\sim 70^\circ$).

and GOES ~ 5 km at this latitude) and the satellite zenith angle (MODIS $\sim 20^\circ$ and GOES $\sim 70^\circ$). Compared to previous observations, the volcanic cloud was starting to form an arc that extends to the NW but overall drifting to the NE. Also, a segment near the volcano can be seen splaying off to the east. In MODIS B31 data, the volcanic cloud is easily detected, consisting of opaque and translucent portions. In the MODIS B31m32 data, the cloud shows variations in its internal structure that are similar to the B31 data but more clearly distinguishes distal portions of the volcanic cloud from weather clouds. The lowest B31m32 data value is -0.7 . The volcanic cloud in the GOES B4 data appears to be more opaque near the volcano and in mid-plume, and then becomes trans-

lucent, blending with weather clouds in distal portions. The more opaque mid-plume signature corresponds with the strongest B4m5 value of the plume at -11.5 . Surprisingly, the GOES split-window signature is an order of magnitude greater than the MODIS split-window signature. The area of the volcanic cloud in the B4 GOES data is approximately three times larger than in the B31 MODIS data. It is unreasonable to expect the volcanic cloud to double in size in 5 min so the difference is probably related to the oblique view of the GOES sensor compared to the nadir view of the MODIS sensor (D. Schneider, AVO, personal comm.), although changes in atmospheric conditions or design and sensitivity differences in the sensors may also have an effect. The area of the

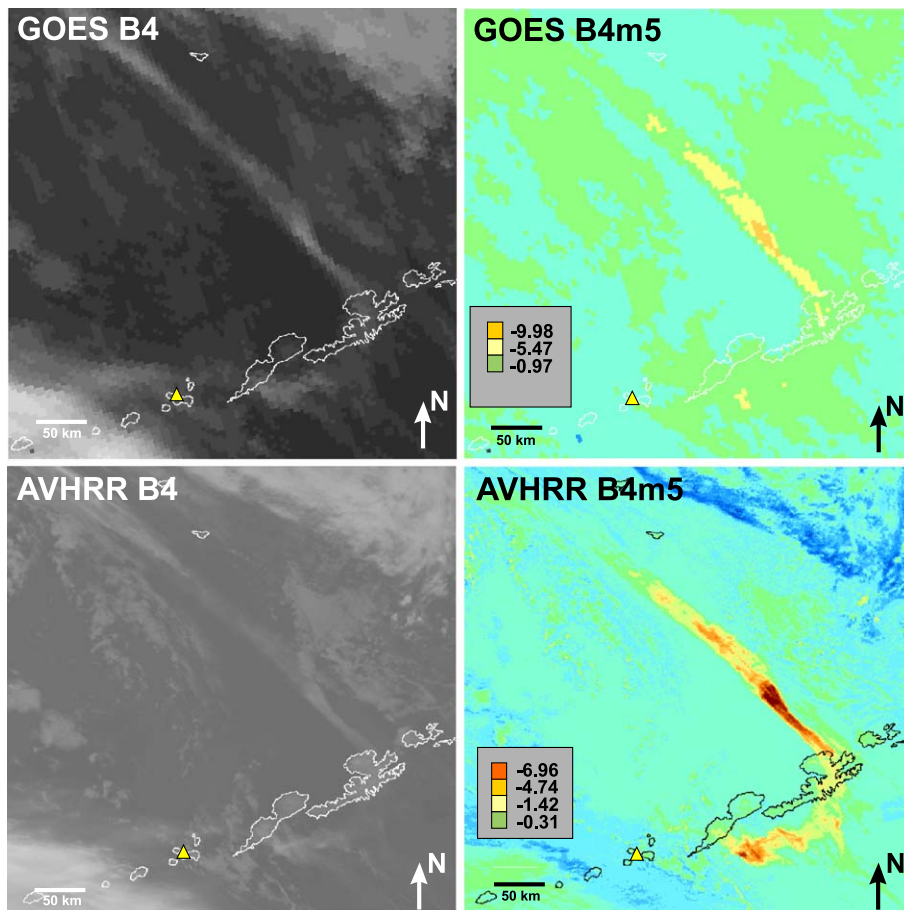


Fig. 6. GOES (0230 UT) and AVHRR (0242 UT) satellite images recorded approximately 12 h after the start of the 19 February 2001 eruption. These images were recorded within 12 min of each other. The volcanic cloud is becoming translucent in the single band 4 data but shows clearly in the B4m5 data. The AVHRR B4m5 shows better detail of internal structures in the volcanic cloud.

volcanic cloud in the split-window MODIS (B31m32) and GOES (B4m5) data are similar although distal portions are more clearly distinguished from surrounding weather clouds in the B31m32 image. Overall, GOES and MODIS data in the 10–12 μm wavelengths are equally effective in detecting the volcanic clouds at this time, although the MODIS data show intricate details in the structure of the volcanic cloud.

The volcanic cloud from the Late Period (Fig. 6) was recorded in GOES (0230 UT) and AVHRR (0242 UT) data approximately 12 h after the start of the eruption and only 12 min apart. The volcanic cloud disconnected from the volcano by 0230 UT. These satellite data show the volcanic cloud continuing to extend to the NW and drifting to the NE. In the GOES and AVHRR B4 data, the volcanic cloud is translucent and difficult to distinguish from weather clouds. The B4m5 data from both satellites detect the volcanic cloud much more clearly than the single band data.

The volcanic cloud in the AVHRR B4m5 data can easily be delineated and the southern end almost extends back to the volcano. Interestingly, the B4m5 signal is stronger in the GOES data (–10.0) compared to the AVHRR (–7.0) but the AVHRR image shows more variation in the ash signal. The area of the volcanic cloud detected in the single-band GOES and AVHRR data are similar. The area of the volcanic cloud measured on AVHRR split-window GOES data is approximately twice as large as on the GOES split-window data. Note that changing the GOES-data map projection from Lambertian Azimuthal to Albers Equal Area to match the AVHRR and MODIS images resulted in re-sampling of the data thereby affecting the number of volcanic cloud pixels and their values.

There are distinct differences in volcanic cloud detection between the four MODIS bands analyzed during the Mid Period (Figs. 7 and 8). These differences are related to the sensitivity of various wavelengths to the composition of the volcanic plume and

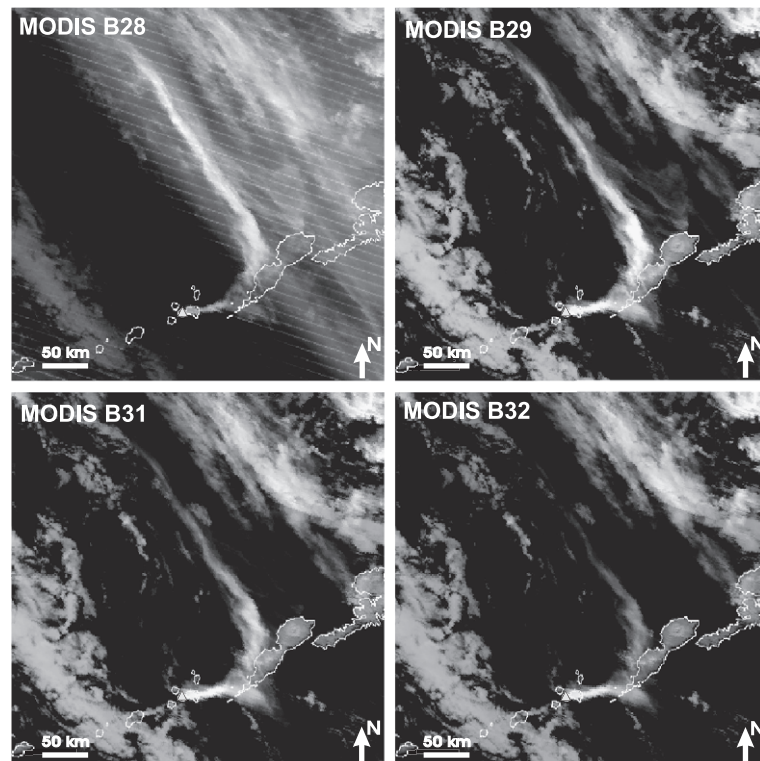


Fig. 7. Thermal infrared MODIS (2310 UT) bands 28, 29, 31 and 32 recorded approximately 9 h after the start of the 19 February eruption. The bands show variation in the detection of the volcanic cloud as a function of wavelength.

meteorological conditions. The intent of this portion of the analysis is to show these variations. The shape and overall extent of the volcanic cloud is similar in each of the bands but opaque and translucent portions vary in extent and position. All four of the bands show variations in the internal structure of the volcanic cloud. Interestingly, B31 and B32 (Table 1 and Fig. 7), which are comparable to GOES and AVHRR thermal infrared wavelengths B4 and B5, were not as effective at detecting the volcanic cloud as B28 and B29 in terms of area. In B31 and B32, the portion of the volcanic cloud near the volcano is easily detected whereas distal portions are translucent and narrow. Band 28 data show the broadest volcanic cloud that

tends to blend with surrounding weather clouds but with a bright, mostly opaque signature throughout its length. Band 29 data shows a mostly opaque signature near Mt. Cleveland and in the middle of the volcanic cloud. Bands 28 and 29 are sensitive to the presence of SO₂ and water vapor (Realmuto, 1995, 2000), and thus the spectral signatures and area measurements of the volcanic cloud will include these constituents. Bands 31 and 32 are more sensitive to volcanic ash. Of the MODIS single channel data analyzed, B28 (7.175–7.475 μm) and B29 (8.4–8.7 μm) detected the largest area of the cloud.

MODIS split-window data show very different aspects of the volcanic cloud (Fig. 8). The volcanic

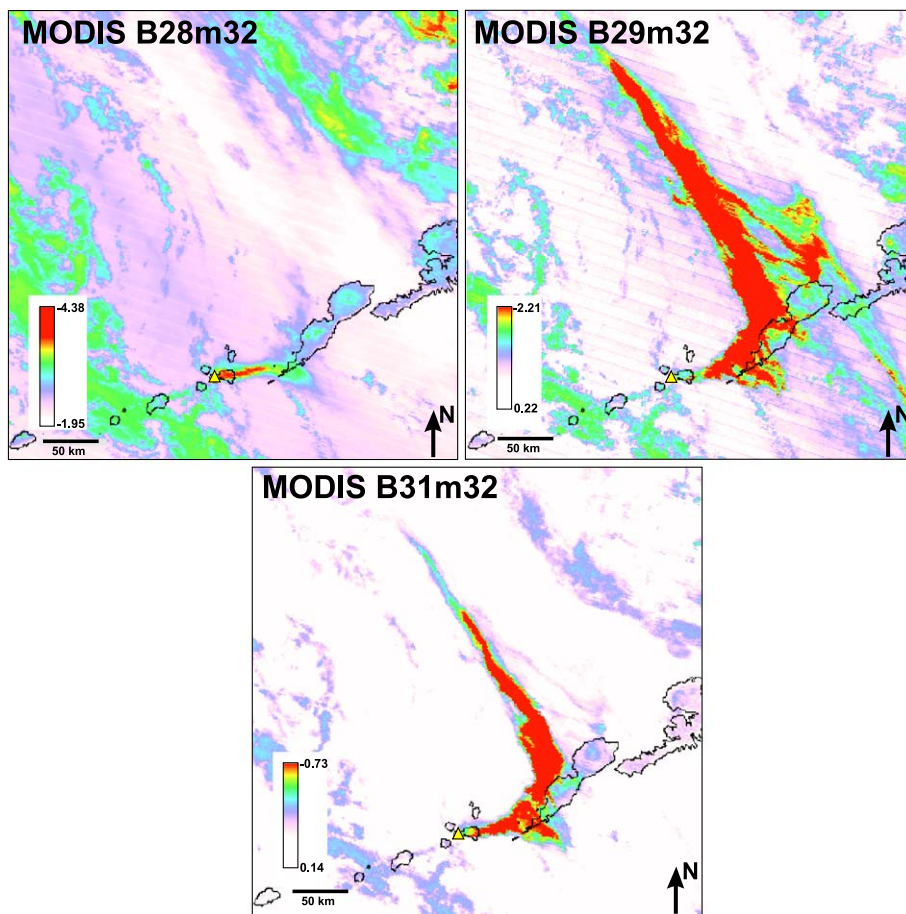


Fig. 8. Split-window MODIS (2310 UT) bands 28m32, 29m32 and 31m32 recorded approximately 9 h after the start of the 19 February eruption. Red indicates areas with the lowest split-window values. B31m32, which is comparable to the conventional B4m5 in GOES and AVHRR data, shows the most detail of internal volcanic cloud structures. B29m32 shows the largest extent of the volcanic cloud but may include weather clouds. B28m32 detected the smallest extent of the volcanic cloud.

cloud in B28m32 is short, extending to the east, and may be SO₂ due to absorption in B28 (Realmuto, 1995), whereas B29m32 and B31m32 data show a volcanic cloud with a similar shape and area to the cloud with a negative signal in the GOES B4m5 data for this period (Fig. 5). B29m32 record the most extensive volcanic cloud of the split-window data analyzed (Table 2) probably due to the detection of ash and SO₂ (Ellrod and Im, 2003; Realmuto et al., 1997). B31m32 appears to show finer internal structural detail compared to the B29m32 data. B28m32 had the strongest split-window signal (−4.4) and B31m32 the weakest (−0.7). For overall split-window data, B29m32 appears to detect the most extensive volcanic cloud probably due to constituents detected while B31m32 appears to best distinguish volcanic clouds from weather clouds for this eruption at this time.

Generally, the split-window technique over the 10–12- μ m range detected the largest extent of the volcanic cloud for most data sets analyzed. However, the area of the volcanic cloud in the MODIS B29m32 data is slightly larger than that detected on the MODIS B31m32 and GOES B4m5 data for the Mid Period. For single-band MODIS data B28 and B29 appear to be the best channels to visually detect the volcanic cloud. The MODIS B28m32, B29m32 and B31m32 all appear to provide information regarding the eruption cloud.

8. Tracking model predictions

The Puff dispersion model (Searcy et al., 1998) was used to predict the shape and movement of Mt. Cleveland eruption clouds (Dean et al., 2002). The simulations were compared with satellite observations, ash fall reports and with pilot reports to validate predictions. The satellite imagery and the model showed that the early volcanic cloud (19 February) extended northwest and southeast of the volcano (Fig. 2). The model indicated that a wind shear at approximately 6-km altitude resulted in this bi-directional extension thereby indicating an approximate height of the early southeast cloud. Approximately 7 h after the start of the eruption, the volcanic cloud was predicted to be over the village Nikolski where ash fell at approximately this time. The simulation for the next

40 h indicated that the cloud would continue to drift to the northeast and the length of the arc-shaped cloud would continue to extend to the northwest and southeast. However, the time sequential GOES imagery (Fig. 9) shows only the northwest extension and northeast drift of the cloud casting doubt on the Puff prediction. However, near San Francisco, 3500 km southeast of the volcano on 22 February, an aircraft Pilot Report (PIREP) from a Boeing 747 states, “particles and strong (sulfur) smell in the cockpit” (Simpson et al., 2002). The timing and position of this report closely matches the Puff simulation, suggesting that the southeast extension of the eruption cloud may be a valid prediction (http://puff.images.alaska.edu/animations/cleve_reanalysis.gif). The CANERM (Simpson et al., 2002; <http://www.cmc.ec.gc.ca/cmc/CMOE/vaac/pph/A-pph.html>) and Hysplit (<http://www.arl.noaa.gov/ready/hysplit4.html>) dispersion models also predicted the southeast extension and movement of the eruption cloud (presentations by B. Stunder and R. Servranckx, Operational Implications of Airborne Volcanic Ash: Detection, Avoidance and Mitigation, Anchorage, Alaska, 7–9 May 2002, organized by G. Hufford, US National Weather Service).

For the 11 March eruption, Puff predicted a v-shaped cloud with its apex at Mt. Cleveland and open to the northeast. The shape of this cloud was due to a wind shear at approximately 8-km altitude with the northern leg of the simulation above 8 km and the southern leg below 8 km. Satellite data showed that only the southern leg of the volcanic cloud was present, indicating that the maximum height of the eruption was less than 8 km at this time. Satellite-derived volcanic cloud temperatures, when compared with atmosphere temperature profiles, indicated an altitude of 7 km, which is close to the model prediction. Also, the satellite data confirmed the northeast movement predicted by Puff.

For the 19 March eruption, Puff predicted that the volcanic cloud would initially drift southeast at all elevations and would turn south approximately 5 h into the eruption. The Puff predictions in general agree with the AVHRR and GOES satellite observations, but the model failed to predict the east–southeast portion of the cloud shown on the images. Also, there were differences in the predictions of the movement of this cloud, depending upon the wind fields

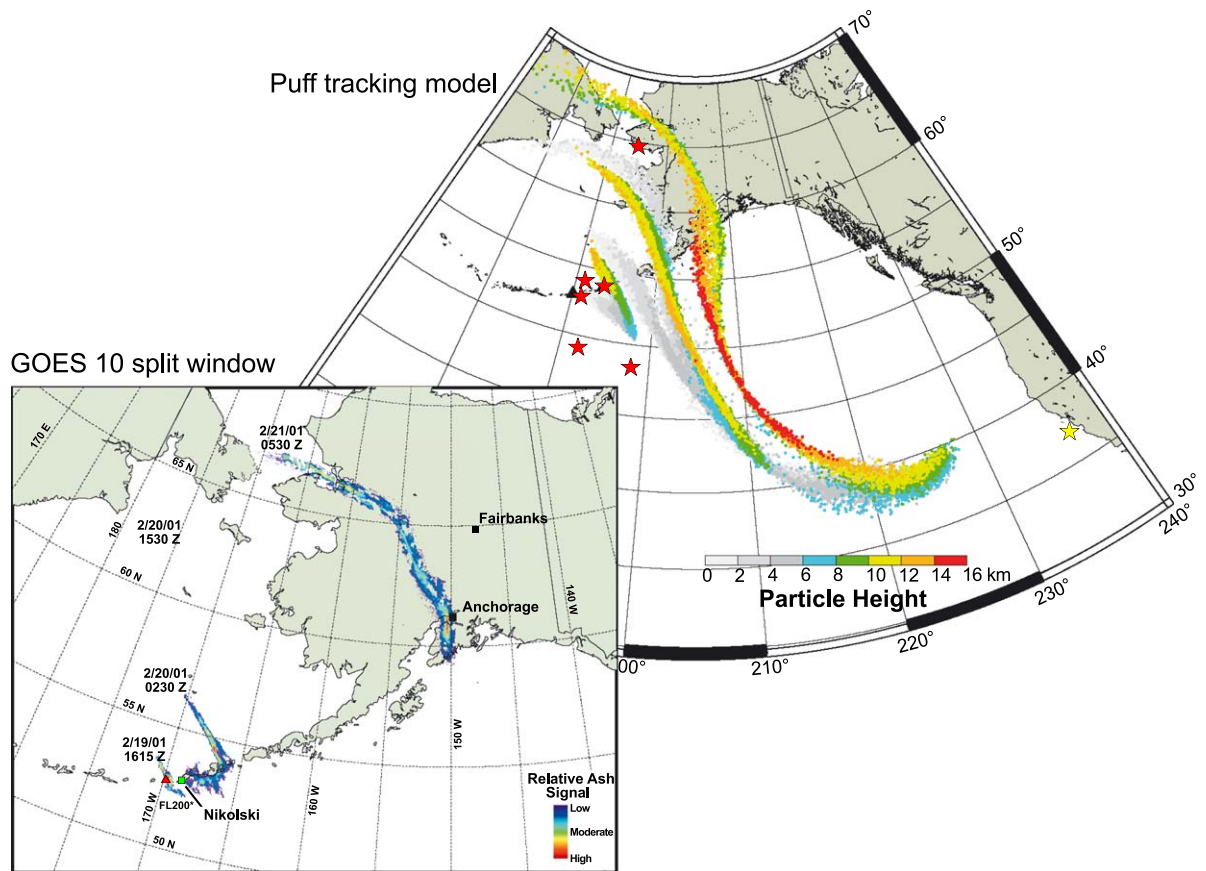


Fig. 9. Puff tracking model results compared to GOES split window imagery of the 19 February eruption cloud. The signal in the split window images and the puff simulations correspond in time to 20 February 0230, 1530 UT and 21 February 0530 UT. The positions of the modeled eruption clouds agree with satellite images north of the Aleutian Islands, but the Puff model suggest that the cloud extended to the southeast beyond 40°N latitude. The red stars indicate the position of aircraft that observed or detected the eruption cloud; the yellow star is the position of an aircraft that reported sulfur and particles in the cockpit.

used. This contrasts with the 19 February event where the model predicted particles where satellite data detected an ash signal as well as areas where no ash signal was present. In this 19 March event, Puff did not predict particles in an area where the satellite data detected an ash signal. This event shows how critical satellite data are for validating models.

9. Thermal anomalies

The first thermal anomaly obvious to analysts accompanied the 19 February explosive eruption. Post-eruption analysis of AVHRR data from 4 Feb-

ruary at 1620 and 1728 UT revealed a possible increase in surface temperature at the summit of Mt. Cleveland (single pixel). This weak signal in nighttime AVHRR band 3 data (3.55–3.93 μm) was 11–12 °C above background and can be difficult to detect during routine monitoring, especially with large variations in the background. The pilot report 2 days earlier of a fresh deposit on the flank of the volcano added some credence to the possible elevated temperature observation (Fig. 10A). No other increases in surface temperatures were observed in these data until the 19 February eruption. Later examination of MODIS data also showed a weak thermal anomaly on 12 February (points A and M in Fig. 10). The lack

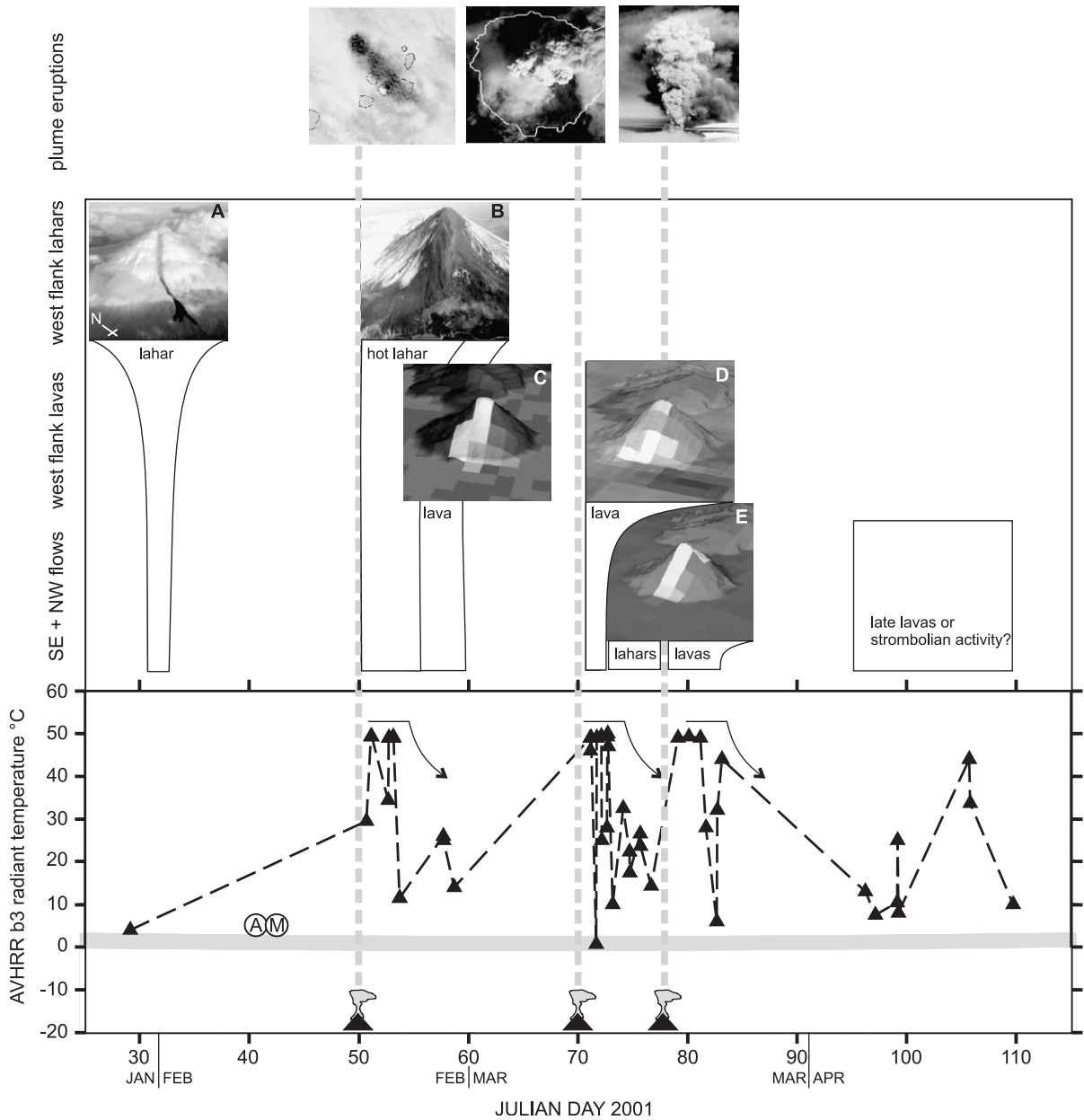


Fig. 10. Time series of thermal anomalies in AVHRR data. The lower graph shows radiant band 3 temperature as a function of Julian days 2001. The gray band at 0 °C represents the background temperature whose width is one standard deviation of normal surface temperatures. The plotted temperatures are derived from thermal anomalies detected by analysts on night-time images during the eruption. The top images show volcanic clouds from the three sub-Plinian events marked as volcanoes on the time scale. The middle images and photographs, labeled A through E, show surface activity and thermal anomalies during the eruption. The AVHRR data (C, D and E) are draped over digital topography to show the change in the thermal signature with time. A and B show lahars resulting in thermal anomalies. C, D and E show thermal anomalies associated with hot lahars and a'a lava flows. Four thermal events were observed, the first three marked by a rapid saturation of the AVHRR sensor, then dropping temperatures as the deposit cooled. The final thermal event shows a different pattern that may suggest late-stage Strombolian activity.

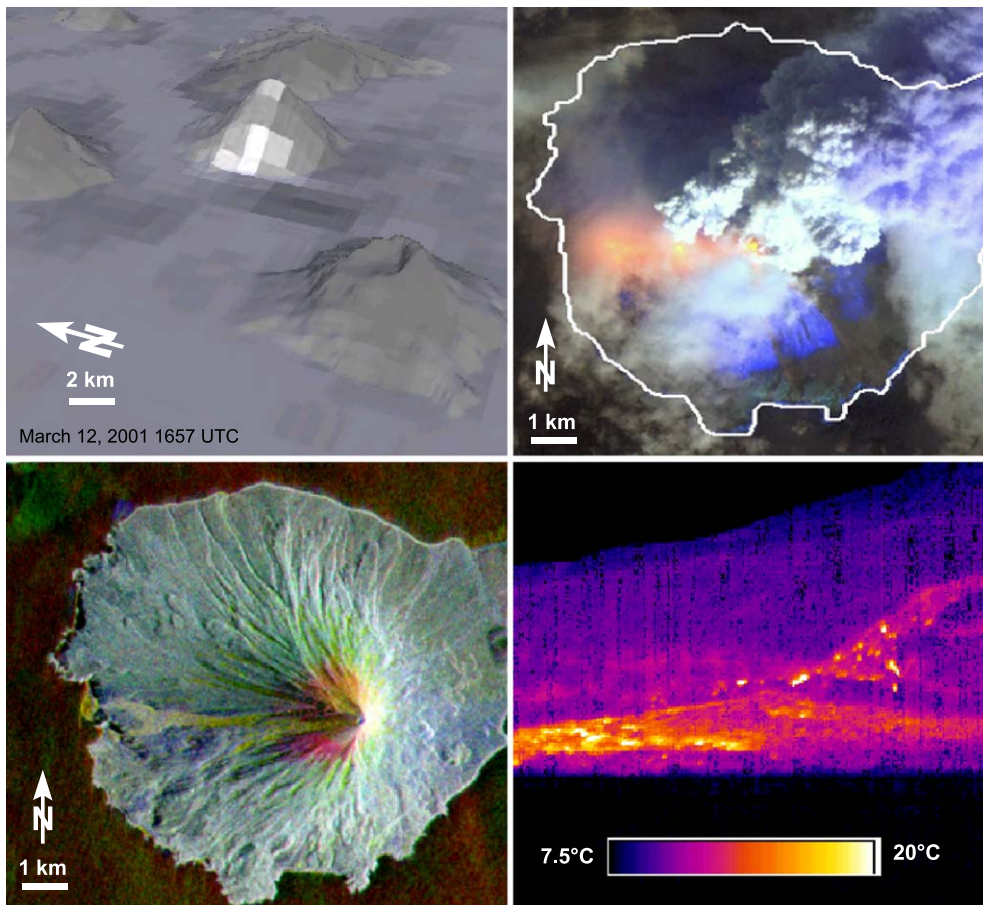


Fig. 11. AVHRR data (above left), Landsat 7 ETM (above right), Radarsat (lower left) and surface FLIR observations (lower right) of the Mt. Cleveland eruption. High spatial resolution of Landsat, RadarSat and FLIR data show the source of thermal anomalies detected on AVHRR data. The AVHRR data recorded on 12 March is draped over a DEM and shows a thermal anomaly extending from the summit to the ocean. The Landsat image shows hot material (orange) flowing down the west slope, snow (blue) and the eruption cloud the day before the AVHRR data was recorded. The RadarSat image shows a new fan along the coast and the flow that resulted from the thermal anomaly. Ground observations and FLIR images recorded during the summer of 2001 and 2002 reveal that the thermal anomaly resulted from a'a lava and hot debris flows. The FLIR image shows the lava flowing down the slope and the hot debris fan. The Landsat image (L71079023_02320010311) is a color composite using the infrared bands in the following channels: B7=red, B5=green and B4=blue. The SAR image is a color composite using data recorded on 2 November 2001 (red and green) and 15 September 2001 (blue). The SAR data have not been terrain corrected.

of additional observed thermal anomalies during this period may be attributed to extensive cloud cover or if the activity were low-level Strombolian, which is episodic, requiring the satellite pass to nearly coincide with an event to record a signal (Dehn et al., 2002). Thus, there is a low probability of recording many thermal anomalies during this time.

A large thermal anomaly (6 pixels at a zenith angle of 4.8°) at the summit was detected in AVHRR data at the time of the first explosive eruption on 19 February.

Within a few days, lava and debris flows extended down the west flank of the volcano to the coast, where a debris fan of hot material was formed (Figs. 10B and 11). Surface temperature and size of the thermal anomaly decreased and were not observed after approximately 1 week.

Thermal anomalies were observed on AVHRR and Landsat data during and shortly after the second and third explosive eruptions on 11 and 19 March (Figs. 10D, E and 11). The Landsat 7 ETM+ image, which

has a 15- and 60-m spatial resolution, recorded the volcanic cloud from the 11 March eruption, and showed a narrow thermal anomaly extending down the west flank of the volcano from the summit to the coast (Fig. 11). These anomalies show some of the characteristics of lavas, saturating the sensor for a period of time, and then cooling rapidly (Dehn et al., 2000). However the period of saturation, often taken to indicate active extrusion (Dehn et al., 2000; Harris et al., 1997), was quite short for each time period. This may suggest small volume lavas with less areal coverage. Since the activity here ranged from Strombolian to debris and then lava flows, often simultaneously, no clear assumptions can be made to calculate lava effusion rate or thermal flux for this eruption (Flynn et al., 2001).

Additional thermal anomalies were observed in April (after Julian Day 95), but these do not clearly follow the patterns known in time series plots of the earlier lavas. The sporadic pattern may represent weak Strombolian activity (Dehn et al., 2000), or warm lahars.

Field observations in September 2001 and 2002 revealed the source of the thermal anomalies on the west flank to be 'a'a lava flow and volcanoclastic debris-flow deposits. Typically, debris flows, sometimes from the collapse of hot molten material near the summit, precede the lavas. The channels created by the debris flows are used by the lava flow, and this sequence of debris overlain by lava was observed at the 1994 deposit, as well as at many older lavas throughout the volcano's stratigraphy. Lahars and lavas were observed radially around the volcano, and must have been responsible for some of the anomalies, particularly those later in the eruption sequence. Over 6 months after the eruption, the debris fan underlying the western 'a'a lava flow was shown to be hot (Fig. 11). AVO geologists have not yet reached the summit to determine the extent of the activity there.

10. Discussion

Excellent satellite coverage from high temporal and spatial resolution satellite data, and dispersion modeling of the volcanic clouds provided detailed information about the sequence of events and types of

activity related to this eruption. The sequence of events were determined using GOES, AVHRR and MODIS data during the crisis, and the types of activity associated with these events were determined using Radarsat and Landsat data, and in situ field observations analyzed after the eruption.

10.1. Eruption precursors

No clear precursors were observed prior to the 19 February eruption. The post-crisis analysis of the data showed weak thermal anomalies labeled as A and M (Fig. 10). Thermal signals are often observed in data prior to explosive eruptions, sometimes resulting from low-level eruptive activity (Dehn et al., 2000, 2002). A Landsat image from 28 June 2000, 6 months prior to the first explosive eruption of Mt. Cleveland, showed a weak volcanic cloud and thermal anomaly at the summit, though there is no reason to suspect that this activity deviates from normal background activity for this volcano. During the last 5 years of AVO monitoring, weak thermal anomalies have been observed twice at Mt. Cleveland (AVO Bimonthly report, September 1997). Field studies after the eruption noted constant steaming and detected weak thermal signals on the order of tens of degrees centigrade using the Forward Looking Infrared Radiometer (FLIR) at the summit during the summer in 2001 and 2002. These could have been post eruption or typical background activity. The original name for this volcano is "Chuginadak", the Aleut Goddess of Fire and the volcano was thought to be her home. It is likely that this steaming has been persistent through historic time, in addition to many eruptions allowing Mt. Cleveland to earn this title in the native culture.

10.2. Volcanic clouds

The eruption at Cleveland provided a good opportunity to compare a clear eruption volcanic cloud in a variety of imagery. The validity of the split-window signal for eruption volcanic clouds has recently been the subject of some debate (Prata et al., 2001; Rose and Mayberry, 2000; Simpson et al., 2000). Instances where detection of volcanic ash in split-window imagery has been both successful and problematic are well documented. For this eruption, the technique worked very effectively. The good signal is probably

the result of the relatively dry sub-arctic atmosphere and what appears to be the fine grain size of the ash (Wen and Rose, 1994). Table 2 summarizes the observations using different image data at different stages in the development of the volcanic cloud on 19 and 20 February. Early in the development of the volcanic cloud (Fig. 2), the primary difference was the result of the wind shear, and what appears to be an earlier low altitude burst from the volcano, which had already become translucent. This portion of the volcanic cloud was not readily visible in the thermal infrared, but was quite apparent in the split-window (B4m5) of the AVHRR data. This volcanic cloud seems to disperse quickly, and as the larger, higher volcanic cloud to the NE evolves it also becomes apparent in the split-window data. This larger volcanic cloud was dense and opaque at the time of the AVHRR image (1643 UT), and hence cannot show a split-window signal, which requires translucent clouds (Rose et al., 2001). The nearest GOES pass is from nearly one half hour before (1615 UT), and shows a smaller areal extent of the volcanic cloud. This is not surprising since volcanic clouds grow rapidly. Even at this earlier time, the SE volcanic cloud had already become translucent, and gives a detectable split-window signal. The NE volcanic cloud had just begun to erupt here and only shows a very small areal extent.

As the volcanic cloud develops, particles disperse, and the cloud goes through the transition from an opaque cloud, best viewed in a single channel (Fig. 5), to a translucent cloud, difficult to detect in a single band (Fig. 6). Here, the split-window data are essential to detect the presence of dry fine ash. At this time, the ability to compare GOES data with the higher spectral and spatial resolution MODIS data presents itself. In the GOES data, with its coarse spatial resolution and oblique view at this latitude, the volcanic cloud is easily detected. As expected, the larger footprint of the pixels in GOES data results in a larger estimation of the area of the volcanic cloud relative to MODIS in all bands. If a pixel shows a signal in GOES data, it accounts for over 25 km² (at the latitude of Mt. Cleveland) compared to a pixel of MODIS data at 1–4 km² (at or away from nadir). As with the data before, the split-window method allows us to delineate the areas containing fine dry ash, and gives larger estimates of volcanic cloud size over single band approaches in both data sets.

MODIS allows us to compare the subtraction of other bands rather than just the AVHRR and GOES B5 (~12 μm) from the B4 (~11 μm). It has been argued (Simpson et al., 2000) that the subtraction of the 12-μm band from the wavelength with the maximum difference in transmittance (near 8.5 μm = MODIS B29) would be more sensitive to the presence of volcanic ash in the volcanic cloud. The MODIS B29m32 data detected a volcanic cloud that was approximately one and a half times larger than that in the B31m32 data, which is in the conventional 11 minus 12 μm range in AVHRR and GOES data (Table 2 and Fig. 8). The increased area in the B29m32 band is probably a result of the inclusion of ash, SO₂ and some weather clouds. Although a qualitative measure, better detail is shown regarding internal structures (i.e. change in the concentration or gradient of ash, volcanic gas or meteorological conditions across the volcanic cloud) in the MODIS B31m32 compared to B29m32 and the GOES data. Granted the size of the structure must be large in order to be visible in GOES and may exceed the dynamic range of single-band MODIS data. Thus, such large signal change might not be as visible as subtle changes in MODIS imagery. However, the MODIS data seem to have a larger threshold value for detecting ash. More examples from other volcanoes with differing composition, grain size and atmospheric conditions, as well as laboratory simulations, will be needed to quantify the relationship of ash concentration to the split-window signal.

For 19 February, the greatest variation in the internal structures of the volcanic cloud was observed in the single-channel B28 and B29 MODIS data. At 7.145–7.475 μm (MODIS B28), better structure is observed farther from the summit, where the volcanic cloud is more diffuse, than on B29 data (8.4–8.7 μm), which seems to respond better to less diffuse ash volcanic clouds closer to the summit. This suggests that the B29 data respond better to larger grain-sizes than band 28. This may be due to the unique cloud composition at this time, and its relative amounts of water vapor and SO₂.

10.3. Lavas and lahars

Thermal anomalies during this eruption were, in most cases, syn-eruptive. In the thermal data time

series (Fig. 10), the signals suggest rapidly cooling lava flows. Without warning, the sensor saturates, holds saturation for a brief time, and then cools rapidly. Other lavas observed in the Aleutians, Hawaii and elsewhere show similar signals, though saturate for a much longer period, up to weeks, presumably due to the much larger volume of the flows and longer periods of effusion (Harris et al., 1997; Mougins-Mark et al., 2000; Patrick et al., 2003). The first photo on 2 February (Fig. 10A) shows a flow extending down the SW flank of the volcano. This is likely not lava because no steaming is visible at the snow-flow boundary, as would be expected for an active lava flow. Further, a lava flow of this size would surely have been detected in thermal imagery. Some warm source near the summit would have to be responsible for snow melt and mobilization of this flow. Small scale Strombolian activity depositing hot spatter on a snow field is likely responsible. In every case observed on the island during field work, lavas (even pre-historic flows) were deposited on top of debris flows. During this eruption, lavas followed on top of debris fans, and it was the lavas that produced the hot signal in satellite data. The lavas were thin (on the order of 10 m or less), short, mostly on the scale of a few km, and not very wide (<100 m). Based on cooling models (Harris and Rowland, 2001; Patrick, 2002), these flows should not have produced saturated signals in satellite sensors for more than a few days.

Field work performed in 2001 and 2002 showed the debris flows to be deposited hot. In September of 2001, over 6 months after the eruption, the debris fan on the western flank was still near 100 °C (Fig. 11). This debris showed little or no structure or bedding, and had to have been formed catastrophically over 1 or 2 days. It added considerable area to the island, several hundred square meters, in an area of deep water off the western shore. There was a large dichotomy in grain size, from sand and smaller to several meter size blocks. Many of the blocks were breadcrust bombs up to 7 m in diameter, some were clearly pieces of lava that had collapsed. The a'ā lava followed on top of the debris flow and never reached the sea. The preceding eruption in 1994 also shows this morphology, with an a'ā lava on top of a debris fan, which exhibits remnant fumarole pipes and mineralization.

Two scenarios suggest themselves for creation of this debris. The first is that the debris flow is a block and ash flow, preceding the lava down the steep slopes of the stratocone. As the lava advances, repeated failure of the flow front would create a deposit, which the trailing flow overrides. However, this suggests multiple collapses, for which there is no evidence in the deposit. Further, this would be an ongoing process as the lava flow slowly moved down the slope. The entire debris deposit was emplaced in less than 2 days while the lava took over a week to creep down the flank of the volcano. No observations of significant flow-front failure of the lava were observed. Finally, the sheer volume of the debris fan is several times larger than the lava flow, and there is no evidence that the lava volume was much larger than the current flow.

The debris could be the result of failure of the thick summit snows under fresh ash and spatter. This would help to explain the catastrophic nature of the deposit, but has difficulty explaining the heat retention. The debris is near 100 °C 6 months after deposition, and in many areas warmer than the a'ā lava nearby and on top. Thus, the temperature during emplacement must have been greater than 100 °C.

It is most likely, that a combination of the above models is responsible for these deposits, and further studies are underway to determine their origin, as they are of importance to the evolution of snow-covered stratocones.

10.4. Distribution of deposits

In general, the tephra from the eruption blew to the east, and the flows, though radial, were concentrated by volume on the western and then eastern flanks. Directly to the south and north, few flows were observed (Figs. 11 and 12). Using RadarSat data, the new deposits can be located due to their lack of vegetation and snow-cover, as well as their increased surface roughness relative to the older deposits. More than half the total area of fresh deposits is located to the west. The remainder spread around the rest of the cone. The largest volumes here are a short lava flow to the SE (Fig. 10E) which appears in AVHRR data, and a cold lahar to the east, which did not cause a thermal anomaly, and sits currently on an undisturbed snow field.

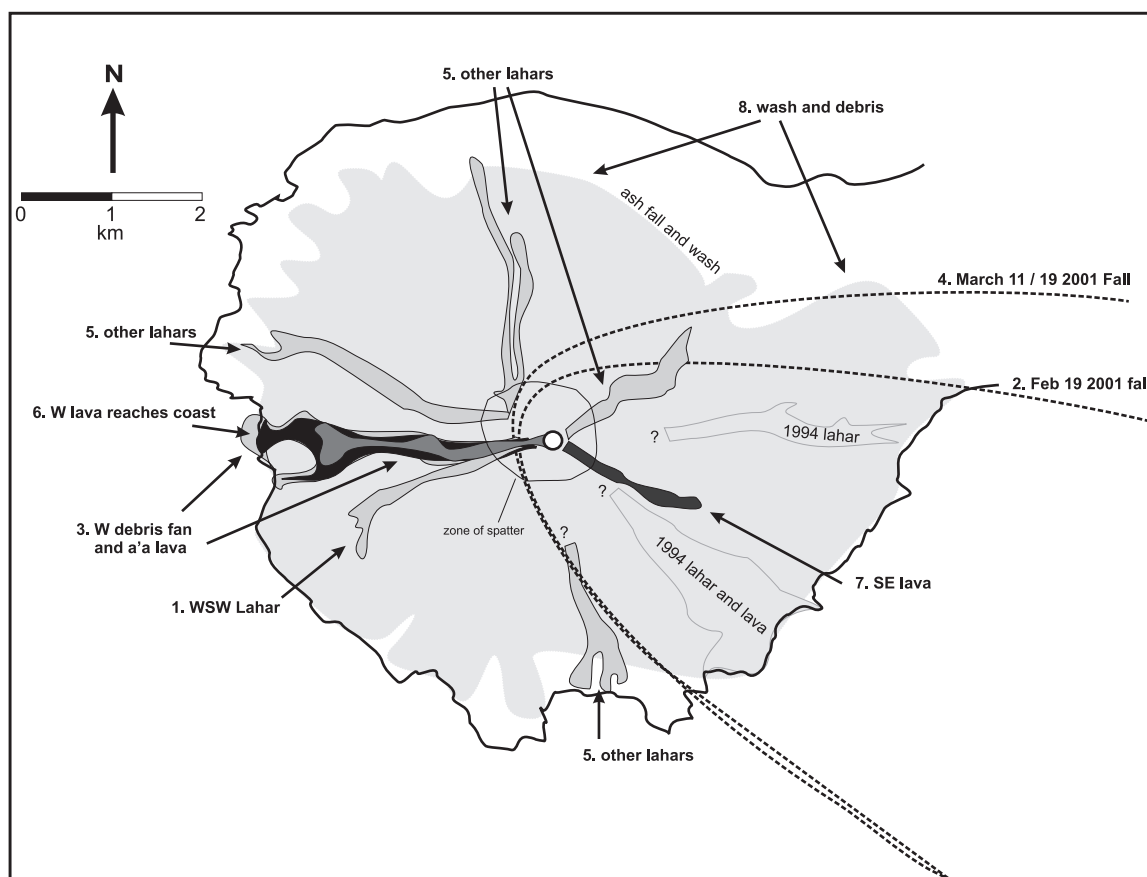


Fig. 12. Sketch map of the deposits from the 2001 eruption. Each is numbered in chronological order from the first lahar to the WSW (1) to the final re-working of the deposits as snow melt occurred (8). The deposits from the last eruption in 1994 deposits are also shown. The map is based on post-eruption Landsat images as well as field observations and samples.

Late stage thermal anomalies in AVHRR data are puzzling. Through April, anomalies were seen, one reaching saturation temperature of the sensor. These anomalies were focused near the summit, or had an east–west trend. This signal is suggestive of Strombolian activity (Dehn et al., 2000); however, it could be the result of a short lava flow and creation of warm debris flows.

A Landsat image acquired in June of 2001 gives the best view of the deposits, though the eastern flank of Cleveland is obscured by clouds. Based on this image and field studies, a sketch map of the deposits was created (Fig. 12). Two areas of ash fall are seen to the east and southeast of the summit on the rest of Chuginadak Island. A darker deposit to the SE is thought to be from the 19 February

eruption, the lighter deposits to the east from the March eruptions. This corresponds to the stratigraphy observed in September, a darker tephra, about 2 cm in thickness was overlain by lighter color tephtras for a total of about 25 cm. The fallout deposit was mostly on snow and vegetation and has since been eroded.

The sequence of deposits began with the WSW lahar, observed on 2 February. This lahar may have resulted from small-scale activity at the summit. The emplacement of the lahar or its source activity were not initially detected in satellite imagery, but re-analysis of these data after the sub-Plinian eruption on 19 February showed a faint thermal anomaly in AVHRR and MODIS data the week following this event. The second event in the eruption was the 19

February sub-Plinian eruption and fall deposit. As part of this event, or immediately afterward, a hot lahar cascaded down the western flank and created a debris fan at the coast. An a'a lava flow slowly followed the path of the debris. The two smaller eruptions on March 11 and 19 created another fall deposit, and more lahars were deposited radially from the summit. After this, the western a'a lava flow reaches its maximum extent, but not the sea due to the large deposit of debris following the largest explosive eruption. It appears that, after this, another smaller a'a lava, observed during field work in 2002, flowed down the SE flank. This flow may be responsible for late stage thermal anomalies observed in AVHRR data. Finally, as the summer arrived, the summit snows melted, fresh ash and old debris were washed down the flank, obscuring the deposition record.

10.5. Puff model predictions

Puff predictions usually result in a volcanic cloud that is more extensive than shown on satellite data. Often input parameters, such as dispersion, are modified to generate a model-result that looks more like the satellite image. In the case of the 19 February Cleveland eruption no “tuning” was performed on the model. An important result from this eruption was input from pilot reports. These reports were incorporated into the model in terms of their aircraft position at the time of the report. In a Puff animation (see Fig. 9 and http://puffimages.alaska.edu/animations/Cleve_021901_76.gif) the aircraft are represented as stars and turn red at the time that they report a condition that could be associated with a volcanic cloud. One interesting report occurred near the California coast where the pilots reported smelling sulfur and noticing particles in the cockpit (Simpson et al., 2002). Initially, this report was disregarded since the satellite data did not show any volcanic clouds even close to that area. However, the Puff model showed particles in that area that coincided in space and time with this pilot report. This situation is also present when Puff was run using re-analysis data, which are based on measured winds instead of forecast winds. It has been common practice to tune model predictions to match the satellite data (considered “ground truth”) by modifying dispersion or other parameters. This incident suggests that tuning models to match satellite data may delete eruption-

related particles that may be meaningful when evaluating the impact of an eruption cloud.

11. Summary and conclusions

Operational GOES and AVHRR satellite data in conjunction with dispersion models and local observations provided excellent information to detect and assess the impact of the Cleveland eruption in real-time during the crisis. The combination of high spectral, spatial and temporal resolution data from operational and the new Earth Observing System satellites proved to be very effective after the eruption for assessing the chronology of events and volcanic processes. The combination of satellite data was able to detect and track the eruption cloud as it formed an arc that extended to 1000 km long to the NW and drifted to the NE across Alaska for over 50 h. These data were used to provide information about the nature of the eruption as well as the location, extent, height and expected motion of the ash cloud. This information was then incorporated into hazard statements issued by AVO to other government agencies and the public as described in the Alaska Interagency Operating Plan for Volcanic Ash Episodes.

The eruption provided an important case study of eruption detection and prediction of volcanic cloud movement, characteristics of eruption clouds, and weather pattern-effects at a remote location. Also, high-resolution Landsat and Radarsat data, and field observations verified that the thermal anomalies observed on high temporal and low spatial resolution data were caused by lava flows, hot debris flows and the formation of a debris fan along the west coast.

Specific points are:

(1) Surprisingly, the ash cloud was detected and tracked on GOES satellite data beyond latitude 66°N for more than 53 h despite its oblique view of the Arctic. The GOES data provided an estimate of the eruption start and end time, and showed the areas of greatest airborne ash concentrations compared to other AVHRR and MODIS data. For the purposes of hazard mitigation, GOES was by far the most useful satellite data set for monitoring the movement of an eruption cloud due to its high temporal resolution and detection capabilities.

(2) GOES, AVHRR and MODIS satellite data showed a volcanic cloud of similar shape and position when comparing nearly concurrent data. The GOES sensor detected volcanic clouds with the largest areal extent, which is probably related to its oblique view and large footprint. MODIS data showed the most variation in volcanic cloud area and intra-volcanic cloud structures as a function of wavelength. Of the MODIS bands analyzed (28, 29, 31 and 32), B28, B29 and split-window B29m32 detected the largest volcanic cloud area. However, single-band data, B28 and 29, and B31m32 showed better detail on the internal structure of the volcanic cloud. Split-window data detected volcanic cloud and eruption cloud areas up to approximately three times larger than single band data at the times analyzed. The split-window technique is still one of the most valuable tools to detect fine, dry, airborne ash.

(3) Dispersion models were capable of predicting the shape and movement of eruption clouds in a very complex wind field for over 53 h. The Puff model predicted the movements of particles to the SE well beyond what satellite sensors detected, as did Hysplit and CANERM. Pilot reports indicate that these predictions may be accurate. Thus, tuning dispersion models to match satellite observations may eliminate valid predictions. However, satellite observations are still critical in validating overall model predictions.

(4) This eruption showed no clear precursor signal detected in satellite data. Though during the eruption satellite data was critical to monitoring and analyzing the activity at the volcano. The thermal signals were typical of small lavas, hot debris flows and possibly Strombolian activity as confirmed by later field work.

Acknowledgements

This work was supported by the U.S. Geological Survey as part of the Volcano Hazards Program, through the Alaska Volcano Observatory, a collaborative effort of the USGS, University of Alaska Fairbanks and the Alaska Geological and Geophysical Surveys. Data, information and observations used in this article were compiled during the Cleveland eruption by all of the AVO staff in Fairbanks and Anchorage. Pilots Burke Mees and Dean Cully and

UAF Professor C. Cahill provided many photographs of the eruption. Diana McGlashan, Nikolski Clinic, collected the ash sample. We are indebted to Kevin Engle who solved all of the image processing and data collection problems. The authors would like to thank Dr. Andy Harris and an unknown reviewer for their editing and valuable suggestions.

References

- Carn, S.A., Oppenheimer, C., 2000. Remote monitoring of Indonesian volcanoes using satellite data from the Internet. *Int. J. Remote Sens.* 21, 873–910.
- Dean, K.G., Servilla, M., Roach, A., Foster, B., Engle, K., 1998. Satellite monitoring of remote sensing volcanoes improves study efforts in Alaska. *Eos Trans.-Am. Geophys. Union* 79, 413, 422–423.
- Dean, K.G., Dehn, J., McNutt, S., Neal, C., Moore, R., Schneider, D., 2002. Satellite imagery proves essential for monitoring erupting Aleutian volcano. *Eos Trans.-Am. Geophys. Union* 83, 241, 246–247.
- Dehn, J., Dean, K.G., Engle, K., 2000. Thermal monitoring of north Pacific volcanoes from space. *Geology* 28, 755–758.
- Dehn, J., Dean, K.G., Engle, K., Izbekov, P., 2002. Thermal precursors in satellite images of the 1999 eruption of Shishaldin Volcano. *Bull. Volcanol.* 64, 525–534.
- D'Amours, R., 1998. Modeling the ETEX volcanic cloud dispersion with the Canadian emergency response model. *Atmos. Environ.* 32 (24), 4335–4341.
- Ellrod, G.P., Im, J.-S., 2003. Development of Volcanic Ash Products Using MODIS Multispectral Data. 12th AMS Conference on Satellite Meteorology and Oceanography, 9–13 February 2003, Long Beach, California, 2003.
- Flynn, L.P., Harris, A.J.L., Rothery, D.A., Oppenheimer, C., 2000. High-spatial-resolution thermal remote sensing of active volcanic features using Landsat and hyperspectral data. In: Mougini-Mark, P., Crisp, J., Fink, J. (Eds.), *Remote Sensing of Active Volcanism*. *Am. Geophys. Union Monograph*, vol. 116, pp. 161–177.
- Flynn, L.P., Harris, A.J.L., Wright, R., 2001. Improved identification of volcanic features using Landsat 7 ETM+. *Remote Sens. Environ.* 78, 180–193.
- Harris, A.J.L., Rowland, S.K., 2001. FLOWGO: a kinetical thermorheological model for lava flowing in a channel. *Bull. Volcanol.* 63, 20–44.
- Harris, A.J.L., Butterworth, A.L., Carlton, R.W., Downey, I., Miller, P., Navarro, P., Rothery, D.A., 1997. Low-cost volcano surveillance from space: case studies from Etna, Krafla, Cerro Negro, Fogo, Lascar, and Erebus. *Bull. Volcanol.* 59, 49–64.
- Harris, A.J.L., Flynn, L.P., Dean, K.G., Pilger, E., Wooster, M., Okubo, C., Mougini-Mark, P., Garbiel, H., Thomber, C., De La Cruz-Reyna, S., Rothery, D., Wright, R., 2000. Real-time monitoring of volcanic hot spots. In: Mougini-Mark, P., Crisp, J., Fink, J. (Eds.), *Remote Sensing of Active Volcanism*. *Am. Geophys. Union Monograph*, vol. 116, pp. 139–159.

- Harris, A.J.L., Matias, O., Flynn, L.P., Rose, W.I., 2004. The evolution of an active silicic lava flow field: a Landsat 7 ETM+ perspective. *J. Volcanol. Geotherm. Res.* 135, 147–168 (this issue).
- Heffter, J., Stunder, J.B., 1993. Volcanic ash forecast transport and dispersion (VAFTAD) model. *Weather Forecast.* 8, 533–541.
- Higgins, J., Harris, A.J.L., 1997. VAST: a program to locate and analyse volcanic thermal anomalies automatically from remotely sensed data. *Comput. Geosci.* 23, 627–645.
- Holasek, R.E., Rose, W.I., 1991. Anatomy of 1986 Augustine Volcano eruptions as recorded by multispectral image processing of digital AVHRR weather satellite data. *Bull. Volcanol.* 53, 420–435.
- Hufford, G., Salinas, L.J., Simpson, J.J., Barsk, E., Pieri, D., 2000. Operational impacts of airborne volcanic ash. *Bull. Am. Meteorol. Soc.* 81, 745–755.
- McNutt, S., 1996. Seismic monitoring and eruption forecasting of volcanoes: a review of the state-of-the-art and case histories. In: Scarpa, R., Tilling, R.I. (Eds.), *Monitoring and Mitigation of Volcanic Hazards*. Springer-Verlag, New York, NY, pp. 99–146.
- Miller, T.P., McGimsey, R.G., Richter, D.H., Riehle, J.R., Nye, C.J., Yount, M.E., Dumoulin, J.A., 1998. Catalog of the historically active volcanoes of Alaska. Open File Rep. U.S. Geol. Surv., 98-582. U.S. Gov. Printing Office, Washington, DC, p. 104.
- Mouginis Mark, P.J., Snell, H., Ellisor, R., 2000. GOES satellite observations of the 1998 eruption of Volcan Cerro Azul, Galapagos Islands. *Bull. Volcanol.* 62, 188–198.
- Neal, C.A., Doukas, M.P., McGimsey, R.G., 1995. 1994 volcanic activity in Alaska: summary of events and response of the Alaska Volcano Observatory. Open-File Rep.-U.S. Geol. Surv., 95-271. U.S. Gov. Printing Office, Washington, DC. 18 pp.
- Patrick, M.R., 2002. Numerical modeling of lava flow cooling applied to the 1997 Okmok eruption: Comparison with AVHRR thermal imagery. Unpublished Master's Thesis. University of Alaska Fairbanks, Fairbanks, Alaska, 141 pp.
- Patrick, M.R., Dehn, J., Papp, K.R., Lu, Z., Moxey, L., Dean, K., Izbekov, P., Guritz, R., 2003. The 1997 eruption of Okmok Volcano, Alaska: a synthesis of remotely sensed imagery. *J. Volcanol. Geotherm. Res.* 127, 87–105.
- Prata, A.J., 1989. Infrared radiative transfer calculations for volcanic ash clouds. *Geophys. Res. Lett.* 16, 1293–1296.
- Prata, A.J., Bluth, G., Rose, W., Schneider, D., 2001. Comments on “failure in detecting volcanic ash from a satellite-based technique”. *Remote Sens. Environ.* 78, 341–346.
- Ramsey, M.S., Dehn, J., 2004. Spaceborne observations of the 2000 Bezymianny, Kamchatka eruption: the integration of high-resolution ASTER data into near real-time monitoring using AVHRR. *J. Volcanol. Geotherm. Res.* 135, 127–146 (this issue).
- Realmuto, V.J., 1995. Volcanic SO₂-High and Moderate Spatial Resolution. EOS IDS Volcanology Team Data Product Document Product #3289, version 3, 20 pp.
- Realmuto, V.J., 2000. The potential use of Earth observation system data to monitor the passive emission of sulfur dioxide from volcanoes. In: Mouginis-Mark, P., Crisp, J., Fink, J. (Eds.), *Remote Sensing of Active Volcanism*. Am. Geophys. Union Monograph, vol. 116. Am. Geophys. Union, Washington, DC, pp. 101–113.
- Realmuto, V.J., Sutton, A.J., Elias, T., 1997. Multispectral thermal infrared mapping of sulfur dioxide volcanic clouds: a case study from the East Rift Zone of Kilauea Volcano, Hawaii. *J. Geophys. Res.* 102, 15057–15072.
- Rose, W.I., Mayberry, G.C., 2000. Use of GOES thermal infrared imagery for eruption scale measurements, Soufrière Hills, Montserrat. *Geophys. Res. Lett.* 27, 3097–3100.
- Rose, W.I., Delene, I., Schneider, D.J., Bluth, D.J., Krueger, A.J., Sprod, I., McKee, C., Davis, H.L., Ernst, G.G.J., 1995. Ice in the 1994 Rabaul eruption cloud: implications for volcano hazard and atmospheric effects. *Nature* 375, 477–479.
- Rose, W.I., Bluth, G.J.S., Schneider, D.J., Ernst, G.G.J., Riley, C.M., McGimsey, R.G., 2001. Observations of 1992 Crater Peak/Spurr Volcanic Clouds in their first few days of atmospheric residence. *J. Geol.* 109, 677–694.
- Schneider, D.J., Rose, W.I., Kelley, L., 1995. Tracking of 1992 eruption clouds from Crater Peak vent of Mt. Spurr Volcano, Alaska using AVHRR. In: Keith, T. (Ed.), *The 1992 eruptions of Crater Peak vent, Mt. Spurr Volcano, Alaska*. U.S. Geol. Surv. Bull. 2139, pp. 27–36.
- Schneider, D.J., Rose, W.I., Coke, L.R., Bluth, G.J.S., Sprod, I., Krueger, A.J., 1999. Early evolution of a stratospheric volcanic eruption cloud as observed with TOMS and AVHRR. *J. Geophys. Res.* 104, 4037–4050.
- Schneider, D.J., Dean, K.G., Dehn, J., Miller, T.P., Kirianov, V.Y., 2000. Monitoring and analysis of volcanic activity using remote sensing data at the Alaska Volcano Observatory: case study for Kamchatka, Russia, December 1997. In: Mouginis-Mark, P., Crisp, J., Fink, J. (Eds.), *Remote Sensing of Active Volcanism*. Am. Geophys. Union Monograph, vol. 116. Am. Geophys. Union, Washington, DC, pp. 65–86.
- Searcy, C., Dean, K., Stringer, W., 1998. PUFF: a high resolution volcanic ash tracking model. *J. Volcanol. Geotherm. Res.* 80, 1–16.
- Simpson, J.J., Hufford, G., Pieri, D., Berg, J., 2000. Failures in detecting volcanic ash from a satellite-based technique. *Remote Sens. Environ.* 72, 191–217.
- Simpson, J.J., Hufford, G.L., Pieri, D., Servranckx, R., Berg, J.S., Bauer, C., 2002. The February 2001 eruption of Mount Cleveland, Alaska: case study of an aviation hazard. *Weather Forecast.* 17, 691–704.
- Wen, S., Rose, W., 1994. Retrieval of sizes and total masses of particles in volcanic ash clouds using AVHRR bands 4 and 5. *J. Geophys. Res.* 99, 5421–5431.
- Yu, T., Rose, W.M.I., 2002. Atmospheric correction for satellite-based volcanic ash mapping and retrievals using “split window” IR data from GOES and AVHRR. *J. Geophys. Res.* 107, 1–16.